Journal of Power Sources 189 (2009) 40–44

Contents lists available at ScienceDirect

Journal of Power Sources

journal homepage: www.elsevier.com/locate/jpowsour

Short communication

Microemulsion preparation and electrochemical characteristics of $LiNi_{1/3}Co_{1/3}Mn_{1/3}O_2$ powders☆

Chung-Hsin Lu*, Yu-Kai Lin

Electronic and Electro-optical Ceramics Laboratory, Department of Chemical Engineering, National Taiwan University, Taipei, Taiwan, ROC

ARTICLE INFO

Article history:
Received 27 June 2008
Received in revised form
19 November 2008
Accepted 9 December 2008
Available online 24 December 2008

Keywords:
Layered structure
Microemulsion
Nanosized particles
Cathode materials

ABSTRACT

Layer-structured $LiNi_{1/3}Co_{1/3}Mn_{1/3}O_2$ was successfully synthesized via a reverse microemulsion (RμE) route. Well-crystallized nanosized (around 45 nm) powders were obtained with calcination at 800 °C. The Rietveld refinement data revealed low degree of cationic displacement in the obtained powders. Within the voltage range of 2.5–4.5 V, the microemulsion-derived $LiNi_{1/3}Co_{1/3}Mn_{1/3}O_2$ delivered 187.2 and 195.5 mAh g^{-1} at room temperature and 55 °C, respectively. The prepared powders were found to exhibit low irreversible capacity and good capacity retention. Microemulsion-derived $LiNi_{1/3}Co_{1/3}Mn_{1/3}O_2$ demonstrated better rate capability than the solid-state derived samples, owing to the reduced particle size and increased surface area. Once the upper cut-off voltage reached 4.6 V, the capacity faded more rapidly than in other operation potential ranges. In this study, the microemulsion process effectively improved the electrochemical characteristics of $LiNi_{1/3}Co_{1/3}Mn_{1/3}O_2$. This soft chemical route possesses a great potential for synthesizing other types of cathode materials with multiple cations.

1. Introduction

In the past decade, $LiCoO_2$ has been used as the predominant cathode material in lithium-ion batteries because of the advantages of ease of production, good rate capability and excellent cycling stability [1]. However, its extensive application is limited owing to various factors such as expensiveness of cobalt, concerns about the thermal stability of charged cathode material in electrolyte, and limited numbers of rechargeable lithium ions in the crystal structure of $LiCoO_2$. To overcome the drawbacks of $LiCoO_2$, many candidate cathode materials have also been developed [2–5]. Among these materials, $LiNiO_2$ and $Li(Ni,Co)O_2$ are the ones with higher discharge capacities and the same crystal structure with $LiCoO_2$. However, their application is also restricted due to the difficulty in synthesizing stoichiometric compounds [6,7]. A new material system, Li–[NiCoMn]–O system, has been developed recently in attempt to replace traditional cathode materials [8,9]. In such a system, $LiNi_{1/3}Co_{1/3}Mn_{1/3}O_2$, is the most unique one because it contains equal molarity of Ni, Co, and Mn. In this compound, Ni, Co, and Mn ions are located in the matrix to form a $[\sqrt{3} \times \sqrt{3}]R30^\circ$ type structure with a $R\bar{3}m$ space group [10]. This material has been demonstrated to possess high discharge capacity, good thermal stability, and excellent cycling stability [11–16].

Most research groups adopted the solid-state-reaction process to prepare $LiNi_{1/3}Co_{1/3}Mn_{1/3}O_2$ powders [10,17,18]. However, $LiNi_{1/3}Co_{1/3}Mn_{1/3}O_2$ derived from the solid-state method faces a problem of significantly irreversible charge/discharge behavior. The irreversible capacity problem may be conquered in two ways: one is to alter the starting materials or heating conditions, and the other is to employ other synthesis methods. Therefore, a microemulsion route was adopted to synthesize $LiNi_{1/3}Co_{1/3}Mn_{1/3}O_2$ powders in this study. The reverse microemulsion process has been developed by our group to synthesize cathode materials for lithium-ion batteries [19–21]. This method has the excellences in controlling particle size and morphology, decreasing nucleation, and lowering reaction temperature for the prepared powders. In this study, nanosized $LiNi_{1/3}Co_{1/3}Mn_{1/3}O_2$ was prepared in attempt to achieve enhanced electrochemical reactivity. The electrochemical performances of the solid-state-reaction and microemulsion derived samples were compared and discussed in detail.

2. Experimental

$LiNi_{1/3}Co_{1/3}Mn_{1/3}O_2$ powders were prepared via a reverse-microemulsion process. Lithium nitrate, nickel nitrate, cobalt nitrate, and manganese nitrate were used as the starting materials. An aqueous solution was prepared by dissolving stoichiometric amounts of the above nitrates in de-ionized water to form the water phase. Cyclohexane was chosen as the oil phase. N-hexyl-alcohol and polyoxyethylene (10) octylphenyl ether (OP-10) were adopted as the co-surfactant and surfactant, respectively. The surfactant and

☆ Presented in 14th IMLB conference.

* Corresponding author. Tel.: +886 2 23651428; fax: +886 2 23623040.
E-mail address: chlu@ntu.edu.tw (C.-H. Lu).

0378-7753/$ – see front matter © 2009 Published by Elsevier B.V.
doi:10.1016/j.jpowsour.2008.12.036

co-surfactant were first added into cyclohexane. The water-to-oil (W/O) ratio was set at 1:10. When the water phase and oil phase were mixed together, stable transparent microemulsion solution was obtained. The water phase and oil phase each served as the discrete phase and continuous phase in the microemulsion solution, respectively. The clear microemulsion solution was dripped into approximately 180 °C hot kerosene using a micro-pump to remove water. For obtaining the precursor powders, the oil solution with micelles was further dried in air at 480 °C for 3 h to remove any residual oil and water. After drying, the precursor powders were ground and further heated to 800 °C at a rate of 1.5 °C min^{-1} in a tubular furnace for various calcination durations to synthesize $LiNi_{1/3}Co_{1/3}Mn_{1/3}O_2$ powders.

The electrochemical analysis was performed using assembled 2032 coin-type cells. The cathode was prepared by mixing $LiNi_{1/3}Co_{1/3}Mn_{1/3}O_2$ powders, KS-6 graphite, carbon black (Super P), and polyvinylidene fluoride (PVDF) binder in a weight ratio of 85:5:2:8, respectively, in N-methyl pyrrolidinone (NMP) solvent. The slurry was then coated onto aluminum foil and dried at 150 °C overnight in a vacuum oven. Lithium metal foil was used as the anode, and a polypropylene separator was employed to separate the anode from the cathode. The electrolyte was prepared by dissolving 1.0 M $LiPF_6$ in 1:1 (by volume) mixture of ethylene carbonate (EC)/diethyl carbonate (DEC). The charge and discharge cycles were recorded in the galvanostatic mode at 40 mA g^{-1} within the potential range of 2.5–4.5 V in a multi-channel battery cycling unit (Arbin BT2000). The cells were tested both at room temperature and 55 °C. The kinetic processes of the cells were determined according to AC impedance using an electrochemical impedance spectra analyzer (EIS300, Gamry 3.1). The amplitude of the inputted AC signal was kept at 10 mV and the frequency range was set between 1 mHz and 0.1 MHz.

3. Results and discussion

3.1. Microemulsion preparation of $LiNi_{1/3}Co_{1/3}Mn_{1/3}O_2$ powders

Fig. 1 shows the X-ray diffraction patterns of RμE-derived $LiNi_{1/3}Co_{1/3}Mn_{1/3}O_2$ powders calcined in air at elevated temperatures. For the precursor powders dried at 480 °C for 3 h (Fig. 1(a)), the XRD pattern revealed the formation of a small amount of layer-structured material, suggesting that the microemulsion process can effectively lower the formation temperature because of the improved compositional homogeneity of the precursors. As the temperature was raised from 600 to 800 °C (Fig. 1(b–d)), the diffraction peaks became sharpened, indicating enhanced degree of crystallinity. The precursor powders was heated at 800 °C and quenched to room temperature. As shown in Fig. 1(d), the diffraction line revealed nearly complete development of the hexagonal structure. With prolonging the calcination time from 0.5 to 3 h (Fig. 1(e–g)), the diffraction patterns remained almost identical with the exception that the peaks became sharper with longer calcination time. Layer-structured $LiNi_{1/3}Co_{1/3}Mn_{1/3}O_2$ with an α-$NaFeO_2$ structure was synthesized after calcination at 800 °C for 3 h.

The Rietveld refinement was used to investigate the structure of RμE-derived $LiNi_{1/3}Co_{1/3}Mn_{1/3}O_2$ powders, and the data are shown in Fig. 2. The reliable parameters shown in Fig. 2 indicated that the proposed model was correct. The displacement degree between lithium and transition metal (Ni) was estimated to be 0.03. The hexagonal lattice parameters of $LiNi_{1/3}Co_{1/3}Mn_{1/3}O_2$ were determined to be $a = 2.861(7)$ Å and $c = 14.244(1)$ Å, which are consistent with the values reported by Ohzuku and co-worker [11]. For RμE-derived $LiNi_{1/3}Co_{1/3}Mn_{1/3}O_2$, the ratio of integrated peak (0 0 3) to peak (1 0 4) was found to be 1.42, and a clear split between

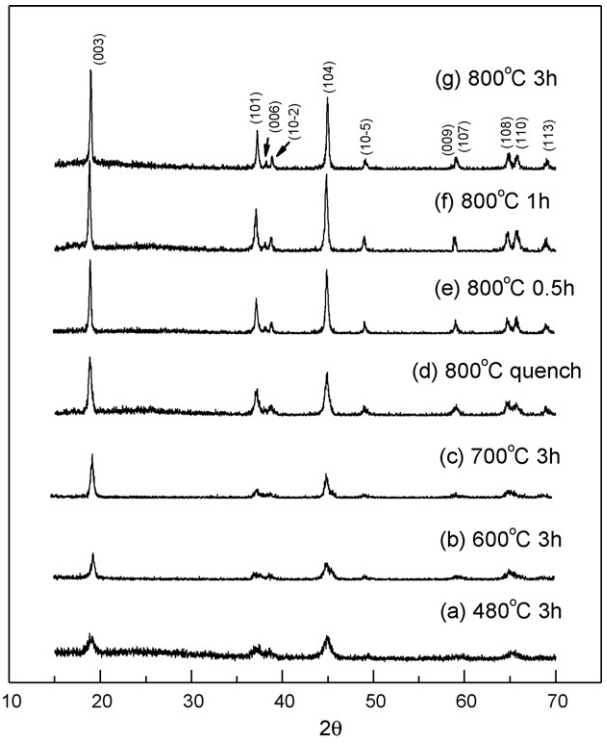

Fig. 1. XRD patterns of microemulsion-derived $LiNi_{1/3}Co_{1/3}Mn_{1/3}O_2$ calcined at elevated temperatures.

peak (1 0 8) and peak (1 1 0) was observed. These results suggest reduced disordering in the host structure of the formed powders. It is demonstrated that the microemulsion process can enhance the compositional homogeneity in the precursors and lower the formation temperature of $LiNi_{1/3}Co_{1/3}Mn_{1/3}O_2$ particles, thereby resulting in a decrease in cation mixing between lithium and nickel ions. The suppressed cation mixing in term helps to improve the electrochemical properties.

Fig. 3 shows the microstructures of RμE-derived $LiNi_{1/3}Co_{1/3}Mn_{1/3}O_2$ powders. Fig. 3(a) displays the TEM image of the powders heated at 480 °C with the particle size of around 12 nm. The bright-field image and selective area diffraction (SAD) pattern for the sample calcined at 800 °C for 3 h are shown in Fig. 3(b). The particle size grew to about 45 nm with 800 °C heating, indicating

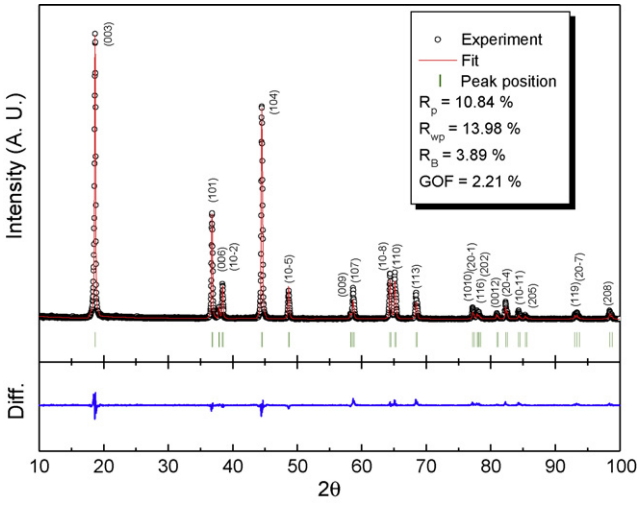

Fig. 2. Rietvelt refinement of microemulsion-derived $LiNi_{1/3}Co_{1/3}Mn_{1/3}O_2$ calcined at 800 °C.

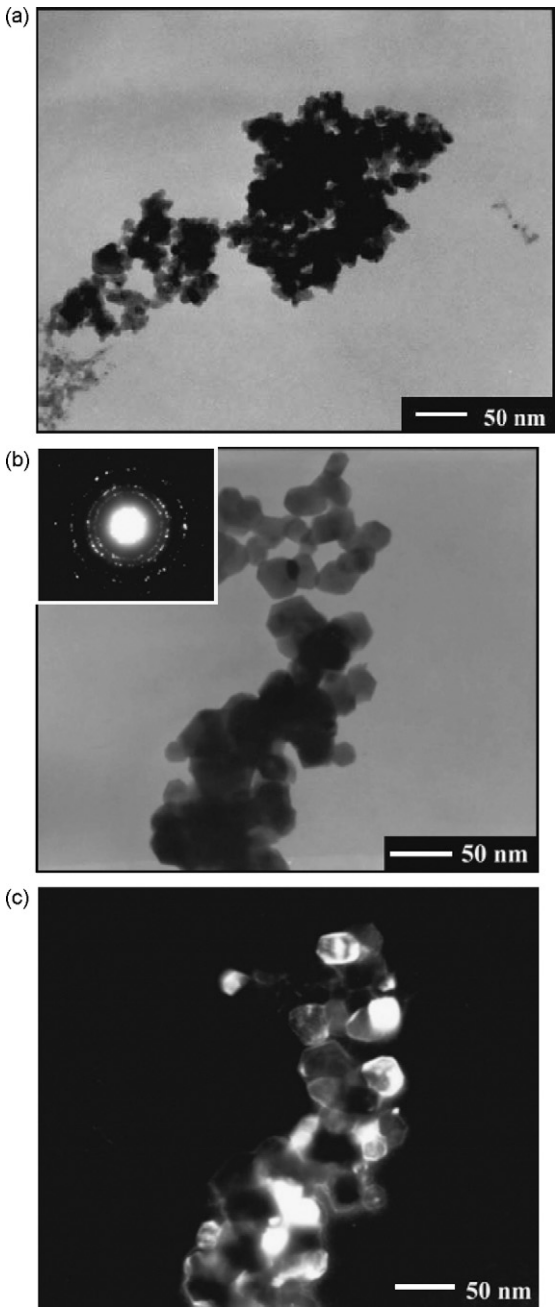

Fig. 3. TEM images of $LiNi_{1/3}Co_{1/3}Mn_{1/3}O_2$ synthesized via the microemulsion route. (a) Precursor dried at 480 °C, (b) bright field image and SAD pattern, and (c) dark field image for 800 °C-heated samples.

that nanosized $LiNi_{1/3}Co_{1/3}Mn_{1/3}O_2$ powders were successfully prepared via the microemulsion process. The SAD pattern exhibited several obvious diffraction rings, revealing that the obtained powders consisted of ultrafine crystallized grains. The corresponding dark-field image as shown in Fig. 3(c) exhibited several lightened particles, indicating that one $LiNi_{1/3}Co_{1/3}Mn_{1/3}O_2$ particle would be a single crystal. In comparison with the solid-state derived samples [22,23], $LiNi_{1/3}Co_{1/3}Mn_{1/3}O_2$ powders obtained in this study had greatly reduced particle size. In the microemulsion process, each reverse micelle acts as an individual reactor, rendering the confinement effect on the constituent reactants. The nanosize and cage-like nature of the microemulsion pose limits on the growth and aggregation of the particles, thereby resulting in the formation of nanosized powders [24].

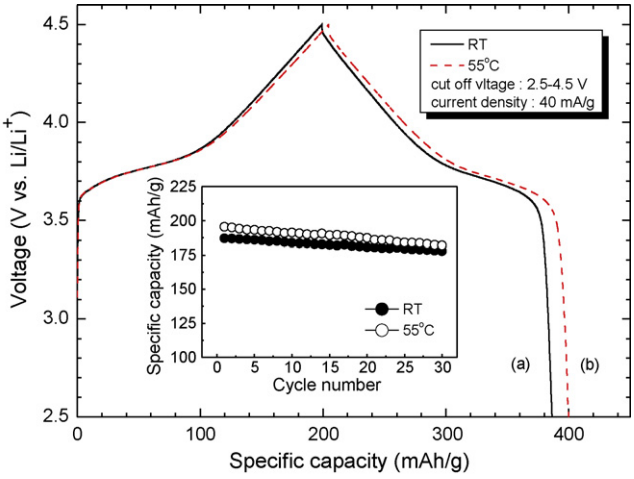

Fig. 4. Charge/discharge curves and specific discharge capacity versus cycle number for microemulsion-derived $LiNi_{1/3}Co_{1/3}Mn_{1/3}O_2$ tested at (a) room temperature and (b) 55 °C.

3.2. Electrochemical analysis of $LiNi_{1/3}Co_{1/3}Mn_{1/3}O_2$ powders

Fig. 4 illustrates the charge and discharge characteristics in the first cycle of RμE-derived $LiNi_{1/3}Co_{1/3}Mn_{1/3}O_2$ calcined at 800 °C for 3 h. The electrochemical properties of the sample were measured between 2.5 and 4.5 V at a constant current density of 40 mA g^{-1} at (a) room temperature and (b) 55 °C. The initial discharge capacities at room temperature and 55 °C were measured to be 187.2 and 195.5 mAh g^{-1}, respectively. The irreversible capacities for the cell tested at room temperature and 55 °C were also calculated to be 5.6% (11.2 mAh g^{-1}) and 4.4% (9 mAh g^{-1}), much smaller than the values for $LiNi_{1/3}Co_{1/3}Mn_{1/3}O_2$ powders prepared via the conventional solid-state process [9,19]. The above phenomenon can be mainly attributed to decreased cation mixing [25]. This kind of cation mixing will probably become more severe if the samples are calcined at high temperatures or in an atmosphere with insufficient oxygen. The microemulsion process can effectively lower the required heating temperature, thereby suppressing the cation mixing occurring at high temperatures. In addition, the nanosized powders prepared via the microemulsion process may exhibit better electrochemical reactivity, thus the irreversible capacity is also reduced. Lithium ions have enhanced diffusion coefficients in the host materials at high temperatures, leading to facilitated kinetic charge transfer reaction and diffusion. Therefore, $LiNi_{1/3}Co_{1/3}Mn_{1/3}O_2$ delivered larger discharge capacity at 55 °C than at room temperature at the same charge and discharge rate. The inset of Fig. 4 shows the relation of specific discharge capacity vs. cycle number for $LiNi_{1/3}Co_{1/3}Mn_{1/3}O_2$ cell at room temperature and 55 °C. After 30 cycles, the discharge capacities at room temperature and 55 °C were 178.3 and 182.2 mAh g^{-1}, respectively, approximating 95% and 93% of the initial values. The prepared powders were found to exhibit good capacity retention in the voltage range of 2.5–4.5 V.

To elucidate the kinetic behavior of lithium-ion transfer, the rate capability tests were carried out. The electrochemical characteristics of the microemulsion-derived nanosized powders as well as the solid-state derived micronsized powders are illustrated in Fig. 5(a and b), respectively. The cells were charged at a fixed current density of 20 mA g^{-1} (0.17 mA cm^{-2}) for each condition. For the microemulsion-derived powders discharged at 20 mA g^{-1} (0.17 mA cm^{-2}), 68% of the theoretical capacity was delivered (189.4 mAh g^{-1}) as shown in Fig. 5(a). With an increase in the current density, the discharge capacity slowly decreased. If the C-rate is defined with respect to 200 mAh g^{-1} [11], the

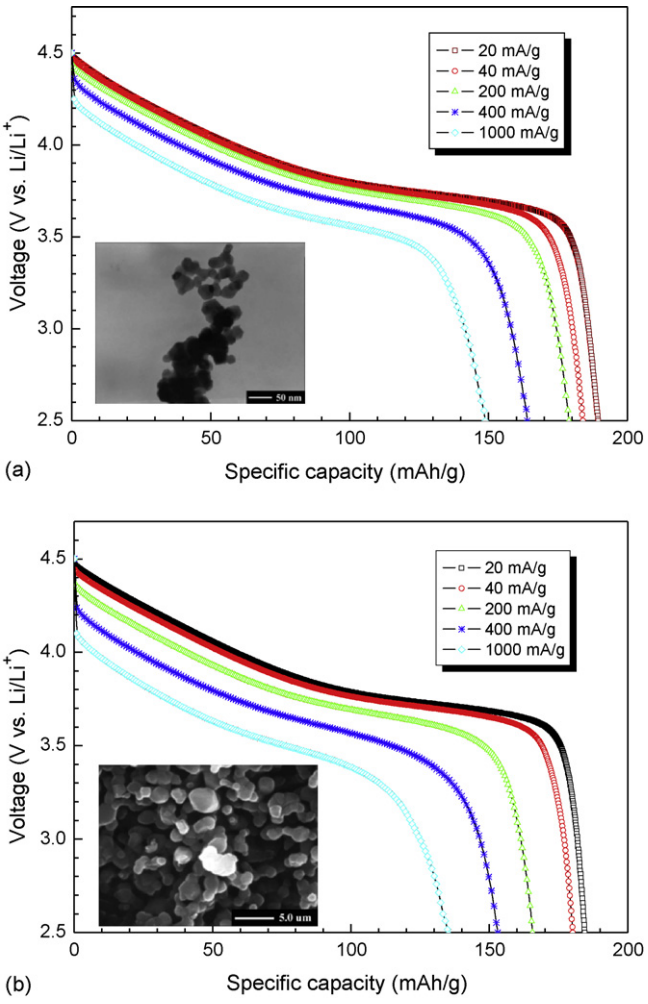

Fig. 5. Discharge curves of $LiNi_{1/3}Co_{1/3}Mn_{1/3}O_2$ tested at various current densities between 2.5 and 4.5 V. The cell was charged at the current density of 20 mA cm^{-2} for each condition. $LiNi_{1/3}Co_{1/3}Mn_{1/3}O_2$ powders were synthesized via (a) the microemulsion process at 800 °C for 3 h and (b) the solid-state process at 1000 °C for 10 h.

microemulsion-derived powders exhibited 178.9 mAh g^{-1} at 1C-rate (200 mA g^{-1}) and 148.8 mAh g^{-1} at 5C-rate (1000 mA g^{-1}). As shown in Fig. 5(b), the solid-state derived powders delivered 184.4 mAh g^{-1} at a current density of 20 mA g^{-1}, and the specific discharge capacity significantly decreased with increasing current density. The capacity of the solid-state derived sample in our study is comparable with the dada reported in literature [26]. At the current density of 200 mA g^{-1}, the discharge capacity was decreased to 165.7 mAh g^{-1}. Once the current densities were increased to 400 and 1000 mA g^{-1}, the discharge capacity were further reduced to 153.0 and 135.2 mAh g^{-1}, respectively. On the other hand, the microemulsion-derived powders had increased surface area and enhanced reactivity due to their nano-scaled sizes. The diffusion length and resistance for lithium ions would be reduced, leading to an improvement in the electrochemical behaviors. The rate capability tests indicate that microemulsion-derived $LiNi_{1/3}Co_{1/3}Mn_{1/3}O_2$ has great potential for high C-rate applications.

Fig. 6 shows the specific discharge capacities of $LiNi_{1/3}Co_{1/3}Mn_{1/3}O_2$ cell charged to various upper cut-off voltages and measured for several cycles. As expected, the discharge capacity increased with increasing upper cut-off voltage. In the voltage range of 2.5–4.0 V, 2.5–4.2 V, 2.5–4.4 V, and 2.5–4.6 V, the first specific discharge capacities of $LiNi_{1/3}Co_{1/3}Mn_{1/3}O_2$ cell were 122.45, 154.63, 177.64, and 208.32 mAh g^{-1}, respectively. As the

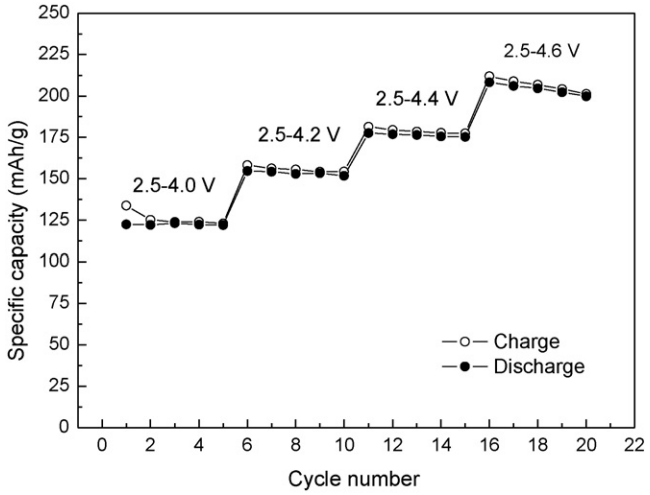

Fig. 6. $LiNi_{1/3}Co_{1/3}Mn_{1/3}O_2$ tested at various potential ranges within a current density of 40 mA g^{-1}.

upper cut-off voltage was below 4.4 V, the $LiNi_{1/3}Co_{1/3}Mn_{1/3}O_2$ cell showed excellent capacity retention since the degradation of discharge capacity was less than 2% after five cycles. However, for the voltage range of 2.5–4.6 V, the discharge capacity faded to 95.89% of its initial value after five cycles. The charge capacities for four voltage stages were 133.9, 158.2, 181.4, and 211.9 mAh g^{-1}, corresponding to 48.2%, 56.9%, 65.3%, and 76.2% of the theoretical capacity (278.0 mAh g^{-1}), respectively. It was reported that the redox reactions of Co^{3+}/Co^{4+} occur when over 67% of lithium ions are extracted from $LiNi_{1/3}Co_{1/3}Mn_{1/3}O_2$ [10]. This implies that once the upper cut-off voltage is below 4.4 V, the capacity is derived from the redox reactions of nickel ions. The capacity fading at a high upper cut-off voltage is considered to be related to the charge compensation of cobalt ions.

Fig. 7 illustrates the impedance curves of $Li/LiNi_{1/3}Co_{1/3}Mn_{1/3}O_2$ cell at various charge stages. The equivalent circuit is also shown in

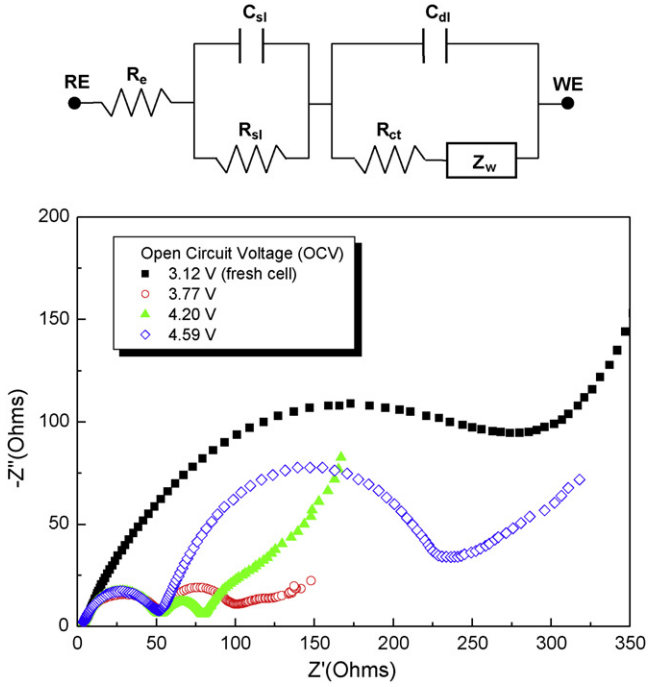

Fig. 7. Electrochemical impedance spectra of $LiNi_{1/3}Co_{1/3}Mn_{1/3}O_2$ cells at various states of charge (SOCs).

Fig. 7 [27]. The cell was first charged to the desired voltage and left in the open circuit condition for 1 h for relaxing the cell potential to a stable value. As shown in Fig. 7, there was only one large arc for the fresh cell with an open circuit voltage (OCV) at 3.12 V. The value on the real axis for this semicircle is regarded as the charge transfer resistance R_{ct}, which approximates 313.1 Ω. Upon the beginning of the charging process, the total resistance of the cell significantly decreased. Based on the equivalent circuit model in Fig. 7, the first arc in the high frequency region was ascribed to the formation of a surface layer, and the second one in the lower frequency region was referred to the impedance derived from bulk electrode and electrode/electrolyte interface. It is noted that R_{sl} seemed independent of the cell voltage and remained unchanged at about 50 Ω until the SEI film was formed. On the other hand, R_{ct} decreased substantially to 59.2 Ω as the voltage dropped from 3.12 to 3.77 V, and then decreased slowly to about 32.5 Ω at 4.2 V. In contrast, while the cell voltage was 4.59 V, the charge transfer resistance increased considerably to about 195.4 Ω.

It was reported that for partially delithiated compound $Li_{2/3}Ni_{1/3}Co_{1/3}Mn_{1/3}O_2$, the Fermi energy level is located in the Ni e_g band [28]. The band gap between the highest occupied bands and the lowest unoccupied bands in $Li_{2/3}Ni_{1/3}Co_{1/3}Mn_{1/3}O_2$ is smaller than that in $LiNi_{1/3}Co_{1/3}Mn_{1/3}O_2$. This implies that the conductivity of $Li_{2/3}Ni_{1/3}Co_{1/3}Mn_{1/3}O_2$ is higher than that of the fully lithiated compound, thereby resulting in a decrease in the charge transfer resistance at 4.20 V as shown in Fig. 7. The charge compensation mechanism for cobalt ions in $Li_{1/3}Ni_{1/3}Co_{1/3}Mn_{1/3}O_2$ during the charging process seems quite complicated and difficult [29]. This demonstrates the importance of selecting proper cut-off voltages in achieving satisfactory electrochemical performance of $LiNi_{1/3}Co_{1/3}Mn_{1/3}O_2$.

4. Conclusions

Reverse-microemulsion derived $LiNi_{1/3}Co_{1/3}Mn_{1/3}O_2$ was successfully prepared in this study. Well-crystallized nanosized powders were obtained with 800 °C heating for 3 h. Based on the Rietveld refinement data, the displacement degree between lithium and transition metal (Ni) was estimated to be 0.03. The initial discharge capacities of $LiNi_{1/3}Co_{1/3}Mn_{1/3}O_2$ at room temperature and 55 °C were 187.2 and 198.4 mAh g^{-1}, respectively. The irreversible capacities at room temperature and 55 °C were estimated to be 5.6% and 4.4%, respectively, much smaller than the values for the solid-state derived samples. Because of the reduced particle size and increased surface area, microemulsion-derived $LiNi_{1/3}Co_{1/3}Mn_{1/3}O_2$ exhibited better rate capability than the solid-state derived samples. Once the upper cut-off voltage was raised to 4.6 V, the capacity faded more rapidly than in other operation potential ranges, which could be related to the redox reactions of cobalt ions. Based on the obtained results, the microemulsion process demonstrated to be an effective method for improving the electrochemical characteristics of $LiNi_{1/3}Co_{1/3}Mn_{1/3}O_2$ powders.

References

[1] T. Nagaura, K. Tozawa, Prog. Batt. Solar Cells 9 (1990) 209–217.
[2] W. Li, J.N. Reimers, J.R. Dahn, Solid State Ionics 67 (1993) 123–130.
[3] T. Ohzuku, A. Ueda, M. Nagayama, Y. Iwakoshi, H. Komori, Electrochim. Acta 38 (1993) 1159–1167.
[4] E. Ferg, R.J. Gummow, A. de Kock, M.M. Thackeray, J. Electrochem. Soc. 141 (1994) L147–150.
[5] M.M. Thackeray, Prog. Solid State Chem. 25 (1997) 1–2.
[6] T. Ohzuku, A. Ueda, M. Kouguchi, J. Electrochem. Soc. 142 (1995) 4033–4039.
[7] I. Saadoune, C. Delmas, J. Solid State Chem. 136 (1998) 8–15.
[8] Z. Lu, D.D. Macneil, J.R. Dahn, Electrochem. Solid State Lett. 4 (2001) A200–203.
[9] T. Ohzuku, Y. Makimura, Chem. Lett. (2001) 642–643.
[10] Y. Koyama, I. Tanaka, H. Adachi, Y. Makimura, T. Ohzuku, J. Power Sources 119–121 (2003) 644–648.
[11] N. Yabuuchi, T. Ohzuku, J. Power Sources 119–120 (2003) 171–174.
[12] I. Belharouak, Y.K. Sun, J. Liu, K. Amine, J. Power Sources 123 (2003) 247–252.
[13] J.J. Choi, A.A. Manthiram, J. Electrochem. Soc. 152 (2005) A1714–A1718.
[14] X.F. Luo, X.Y. Luo, X.Y. Wang, L.L. Liao, S. Gamboa, P.J. Sebastian, J. Power Sources 158 (2006) 654–658.
[15] Y. Fujii, H. Miura, N. Suzuki, T. Shoji, N. Nakayama, J. Power Sources 171 (2007) 894–903.
[16] W.W. Zhang, H.X. Liu, C.C. Hu, X.J. Zhu, Y.X. Li, Rare Metals 27 (2008) 158–164.
[17] K.M. Shaju, G.V.S. Rao, B.V.R. Chowdari, Electrochim. Acta 48 (2002) 145–151.
[18] Z. Wang, Y. Sun, L. Chen, X. Huang, J. Electrochem. Soc. 151 (2004) A914–921.
[19] C.H. Lu, P.Y. Yeh, J. Mater. Chem. 10 (2000) 599–601.
[20] C.H. Lu, Y. Lin, J. Mater. Res. 18 (2003) 552–559.
[21] C.H. Lu, H.C. Wang, J. Electrochem. Soc. 152 (6) (2005) C341–C347.
[22] T. Ohzuku, H. Komori, K. Sawai, T. Hirai, Chem. Express 5 (1990) 733–736.
[23] W. Li, J.C. Currie, J. Electrochem. Soc. 144 (1997) 2773–2779.
[24] A.J. Zarur, J.Y. Ying, Nature 403 (2000) 65–67.
[25] S. Jouanneau, K.W. Eberman, L.J. Krause, J.R. Dahn, J. Electrochem. Soc. 150 (2003) A1637–1642.
[26] L. Zhang, X. Wang, T. Muta, D. Li, H. Noguchi, M. Yoshio, R. Ma, K. Takada, T. Sasaki, J. Power Sources 162 (2006) 629–635.
[27] M.G.S.R. Thomas, P.G. Bruce, J.B. Goodenough, J. Electrochem. Soc. 132 (1985) 1521–1528.
[28] M.G. Kim, C.H. Yo, J. Phys. Chem. B 103 (1999) 6457–6465.
[29] W.S. Yoon, C.P. Grey, M. Balasubramanian, X.Q. Yang, D.A. Fischer, J. McBreen, Electrochem. Solid State Lett. 7 (2004) A53–55.